ACS Sustainable Chemistry & Engineering

pubs.acs.org/journal/ascecg

Research Article

A Facile Route to Efficient Water Oxidation Electrodes via Electrochemical Activation of Iron in Nickel Sulfate Solution

Shiyu Liu, Jian Zhang, Hao Wang, Tewodros Asefa,* and Xiaoxi Huang*

Cite This: *ACS Sustainable Chem. Eng.* 2020, 8, 15550−15559

Read Online

ACCESS | Metrics & More | Article Recommendations | Supporting Information

ABSTRACT: The oxygen evolution reaction (OER) is an important half reaction in many electrochemical energy conversion processes, such as water splitting and carbon dioxide reduction. However, new, scalable and more efficient synthetic methods to inexpensive OER electrocatalysts are currently needed in order to develop water electrolyzers and carbon dioxide reduction cells on large scale. To this end, we here report efficient free-standing FeNi-based electrocatalysts for OER derived from iron, one of the most Earth-abundant metals, by a facile potential cycling synthetic method in an aqueous $NiSO_4$ solution. The optimized catalyst requires a low overpotential of 236 mV to catalyze OER with a current density of 10 mA/cm^2 in 1.0 M KOH solution. More importantly, this free-standing water-oxidation electrode can maintain a current density of 100 mA/cm^2 for more than 72 h. During the course of the electrochemical activation, both cathodic reduction and anodic oxidation are found to play important roles in the surface reconstruction of metallic iron into electrocatalytically active FeNi-based bimetallic hydroxide nanosheet arrays for OER electrocatalysis. This inexpensively fabricated OER electrode prepared from iron has a great potential to reduce the overall cost of water electrolyzers and other related renewable energy systems.

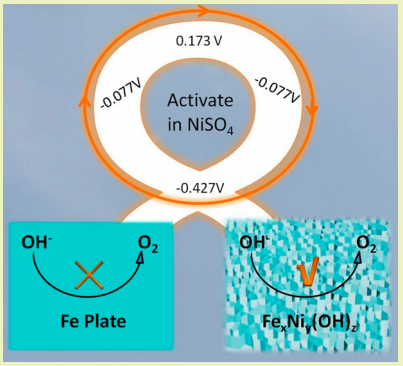

KEYWORDS: *Electrocatalysis, Oxygen evolution reaction, Potential cycling, Electrochemical activation, Iron*

INTRODUCTION

Clean energy technologies continue to attract much attention because they have important roles to play in solving environmental problems and building a sustainable future. Renewable energy-powered water electrolyzers comprising the oxygen evolution reaction (OER) and the hydrogen evolution reaction (HER) are among such promising technologies since they can produce hydrogen (a clean fuel) from water. Owing to the multiple electron-transferring steps involved in it, OER is a difficult half-reaction to carry out; however, it is the most important one governing the overall performances of water electrolyzers.[1−3] Thus, intensive research efforts have recently been directed to the development of efficient OER electrocatalysts, with low overpotentials and improved durability. Of particular interest have been FeNi-based materials, especially their oxyhydroxides, as they are found to effectively electrocatalyze the OER in alkaline solutions.[4−7]

To make OER electrocatalysts both active and durable, fabricating them in free-standing forms rather than in powdered forms helps, because the former do not require binders and can be used directly as electrodes in electrolyzers. The latter in contrast need additional polymer binders to help them stick to conducting substrates and form OER electrodes. Besides, the technical inconvenience, the oxygen bubbles generated by OER can remove the binders as well as the active catalysts, causing the deactivation of the OER electrodes.

Free-standing FeNi-based OER electrodes are predominantly synthesized by hydrothermal treatment,[8−12] electrochemical processes,[13−16] sputtering,[17] and corrosion engineering.[18] Among these synthetic strategies, electrochemical synthetic processes are advantageous since they entail a short reaction time, an ambient temperature and pressure, and simple synthetic set-ups. In addition, they can easily be tweaked (for example, by changing the applied potential or the current density) to improve the structures and compositions of films deposited on substrates and thereby the properties of the electrodes. Conversely, the other methods involve relatively complicated procedures, time-consuming synthetic steps, or high temperatures. For example, hydrothermal synthesis of OER electrodes is generally performed by treating the materials in autoclaves at elevated temperatures for a long time.[19,20] Consequently, the other methods are relatively less conducive for practical applications.

In electrochemical synthesis of OER electrodes, materials such as titanium,[21] nickel foam,[13−15,22] carbon cloths or carbon fiber paper,[23] and noble metals[24] are frequently selected for

Received: June 24, 2020
Revised: July 29, 2020
Published: August 10, 2020

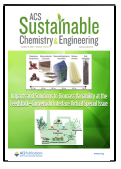

electrodeposition due to their high conductivity and relative stability. On the contrary, despite its low cost, iron is not as widely used as a substrate to synthesize OER electrocatalysts via electrodeposition because it is more susceptible to oxidation in various electrolytes. Moreover, only a few examples involving iron-based OER electrodes synthesized by other methods can be found in the literature.[18,25−27] In one example, a corrosion engineering method using an iron substrate was demonstrated to produce an electrode that is able to catalyze OER at 1000 mA/cm^2 for more than 6000 h.[18] However, the corrosion process still took as long as 12 h to generate the required electrode. In a second example, surface-modification was used to produce iron-based electrode that can serve as an OER catalyst at 10 mA/cm^2 for more than 1000 h;[25] however, the surface modification process involved multiple steps and an elevated temperature.

In this work, we introduce a simple one-step electrochemical method that activates the surfaces of an iron plate in 30 min at room temperature to produce nanostructured FeNi bimetallic hydroxide nanosheet that can serve as efficient and stable electrocatalyst for OER. The resulting electrode requires an overpotential of 236 mV to electrocatalyze OER with a current density of 10 mA/cm^2. We also propose the mechanism that leads to the electrochemical activation of an iron plate into this FeNi-based catalyst. The results show that both cathodic reduction and anodic oxidation in the presence of oxygen are essential to convert an iron plate into an effective OER electrode. The ease of the synthetic procedure and the high abundance and inexpensiveness of the substrate (i.e., iron) make this OER electrode highly appealing for practical water electrolyzers.

EXPERIMENTAL SECTION

Chemicals and Reagents. Iron plate (thickness: 0.3 mm, 99.99% purity) was purchased from Qinghe Guantai Metal Materials Co., Ltd. Nickel sulfate hexahydrate ($NiSO_4·6H_2O$, 99.9% metals basis), potassium sulfate (K_2SO_4, 99.99% metals basis), and potassium hydroxide (KOH, 99.99% metals basis) were purchased from Shanghai Aladdin Biochemical Co., Ltd. Deionized water (≥18.2 MΩ cm), which was purified by Aquaplore 2S system, was used for all experiments.

Electrochemical Activation Method. An iron plate (size: 0.5 cm × 5 cm) was polished with a fine sandpaper (3M) and washed with ethanol several times by ultrasonication to clean its surface. The electrochemical activation of the iron plate was carried out in a three-electrode cell using 8 mL of 0.1 M $NiSO_4$ as electrolyte at room temperature. The pH of the electrolyte was 5.6. The iron plate was directly used as a working electrode (WE). Prior to this, a hot melt adhesive was used to cover the iron plate leaving ca. 0.2 cm^2 exposed. A graphite carbon rod and a saturated calomel electrode (SCE) were used as counter electrode (CE) and reference electrode (RE), respectively.

The electrochemical activation of the iron plate was conducted with cyclic voltammetry (CV) in a potential range of −1.0 to −0.4 V vs SCE for 15 cycles at a scan rate of 10 mV/s. The activated electrode was named as FeNiRedox. The suffix "Redox" indicates the involvement of a redox process (reduction and oxidation) for the synthesis of this electrode. For comparison, two other electrodes were prepared using different potential windows, namely, from −1.0 to −0.65 V (a reduction window) and from −0.65 to −0.4 V (an oxidation window). The resulting electrodes were named as FeNiRed and FeNiOx, respectively. After electrochemical activation, the electrodes were all rinsed with deionized water, and any residual water on them was removed with filter papers through capillary forces. To convert the potentials in RHE scale, the following eq (eq 1) was used

$$E_{RHE} = E_{SCE} + 0.241\ V + 0.0592 \times pH \quad (1)$$

Characterizations. The morphology and structure of the electrodes were characterized by a field emission scanning electron microscope (SEM) (SU-70, Hitachi) and a transmission electron microscope (TEM) (JEM F200, JEOL). Contact angles of the electrodes were measured with a contact angle meter (Theta, Biolin Scientific) using a drop of 1 M KOH solution (4 μL). Inductively coupled plasma atomic emission spectroscopy (ICP-OES) was performed with an Agilent 720ES ICP spectrometer. X-ray photoelectron spectroscopy (XPS) was performed with a K-Alpha XPS instrument (Thermo Fisher Scientific) with a monochromatic X-ray source (mono Al Kα, $h\nu$ = 1486.6 eV). The energy scale of the spectrometer was calibrated using the XPS peak of C 1s (at 284.8 eV) of an adventitious carbon present on the sample. X-ray diffraction (XRD) patterns were obtained with a Bruker D8 Advance diffractometer.

Electrochemical Measurements. All electrochemical measurement were conducted in a cell containing three-electrodes using a PARSTAT MC potentiostat (Princeton Applied Research). The iron-based electrodes fabricated via surface activation, a Hg/HgO electrode, and a graphitic carbon rod were used as working electrodes (WEs), a reference electrode (RE), and a counter electrode (CE), respectively. Linear sweep voltammetry (LSV) curves were collected in 1 M KOH solution at a scan rate of 1 mV/s to evaluate the catalytic activities the iron-based electrodes for OER. The Tafel plots were obtained at a lower scan rate of 0.5 mV/s. Electrochemical impedance spectroscopy (EIS) was performed at a potential of 1.55 V vs RHE under OER condition in a frequency range of 10^4 to 10^{-2} Hz and using an AC voltage with an amplitude of 5 mV. The system's resistance was estimated from a single point impedance measurement after compensating it for 85% *iR*-drop.

The Hg/HgO RE was calibrated by following a previously reported method.[28] Two Pt sheets were polished and cycled from −2 V to +2 V in H_2SO_4 solution (0.5 M) for 2 h to clean their surfaces. The two cleaned Pt electrodes were used as a WE and a CE, respectively. An aqueous solution of KOH (1 M) was bubbled with high purity H_2 gas for, at least, 30 min prior to the calibration. LSV curve at a low scan rate of 0.5 mV/s was obtained to find the potential that gives zero current. On the basis of the LSV curve (see in Figure S1), the potential corresponding to zero current was found to be −0.925 V vs Hg/HgO. Accordingly, the measured potentials were converted to RHE scale by using eq 2 below

$$E_{RHE} = E_{Hg/HgO} + 0.925\ V \quad (2)$$

Electrochemically active surface areas (ECSA) of the catalysts were determined by measuring their double layer capacitances (C_{dl}).[18,21] Several CV measurements were first conducted in the non-Faradaic potential window between 1.125 to 1.225 V vs RHE at different scan rates (50, 25, 10, 5, and 1 mV/s). The difference between half of the anodic and half of the cathodic current densities ($j_{anodic} - j_{cathodic}$) at 1.175 V was then plotted against scan rate. The slope of the fitted line was taken as the value of C_{dl}. ESCA of each material was then obtained by dividing the value of C_{dl} with the specific capacitance of the material, which is taken as 0.04 mF/cm^2.[18,21]

To quantify the gaseous product produced during catalytic OER, the water displacement method was used. From the measured volume of gaseous product, the amount of oxygen (O_2) was determined based on the ideal gas law. The presence of O_2 in the product was confirmed by a gas chromatography (GC) instrument (Agilent 7890B) equipped with a thermal conductivity detector (TCD).

Calculation of Catalytic Turnover Frequencies (TOFs) of Electrodes. TOFs of the electrodes was calculated to compare their intrinsic electrocatalytic activities with one another.[21] ICP-OES was used to measure the amounts of active catalysts, $Fe_xNi_y(OH)_z$, present on the electrodes. ICP-OES was specifically used to measure the amount of nickel on the electrodes. And XPS was used to determine the atomic ratios of Ni and Fe on the surfaces of the electrodes. The TOF of each electrode then calculated according to the following equation (eq 3)

https://dx.doi.org/10.1021/acssuschemeng.0c04666
ACS Sustainable Chem. Eng. 2020, 8, 15550−15559

$$\text{TOF} = I/(4 \times \text{F} \times n) \quad (3)$$

where I is the current measured at a given potential, 4 represents the number of electrons transferred during the OER to form one molecule of O_2, F is the Faraday constant, and n is the number of moles of the total Fe and Ni in $Fe_xNi_y(OH)_z$.

Calculation of Catalytic Mass Activity. The mass activity (in A/g) of the electrocatalysts was calculated by normalizing the measured current (I) with the mass (m) of total Fe and Ni in $Fe_xNi_y(OH)_z$ loaded on the electrode using the following equation, eq 4.[29,30]

$$\text{mass activity} = I/m \quad (4)$$

RESULTS AND DISCUSSION

The electrochemical activation of an iron plate is performed in a conventional three-electrode cell through cyclic voltammetry (CV) (Scheme 1). The procedure is detailed in the Experimental section above. The optimized freestanding electrode is synthesized by conducting 15 cycles of CV in 0.1 M $NiSO_4$ solution under ambient atmosphere from −427 to 173 mV vs RHE at a scan rate of 10 mV/s (*vide infra*). (Note that all measured potentials are reported with respect to RHE unless mentioned otherwise.) The overall CV cycling time needed to produce this optimal electrocatalyst is only 30 min. After the potential cycling, a dark film is observed on the surface of the iron plate (see Figure S2). So most of the discussion below will focus on the electrodes obtained with 15 CV cycles.

Scheme 1. Illustration for the Synthesis Processes Leading to Iron-Based Electrodes for OER via Activation of Iron Plates through CV in $NiSO_4$ Solution

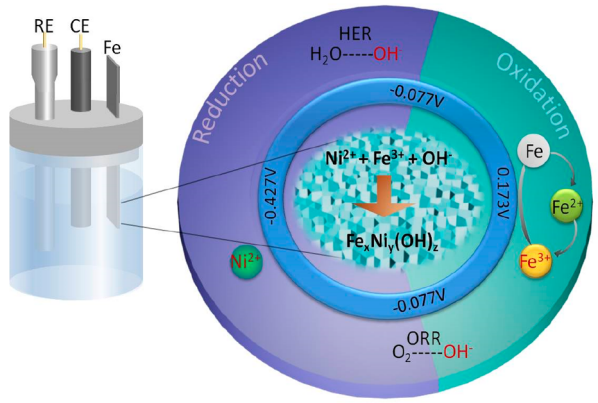

As shown in Figure 1A, the anodic oxidation current in the potential window of −77 to 173 mV increases rapidly as the CV cycles go from 1 to 12 but becomes somewhat stable thereafter. This current corresponds to the oxidation of surface Fe atoms into Fe^{2+} and Fe^{3+} species. On the other side, in the sweeping potential window between −427 and −77 mV, a cathodic reduction peak starts to show up but then gradually diminishes, as indicated by the black arrow in Figure 1A. The peaks in the potential window between −320 to −240 mV are ascribed to the reduction of oxidized Fe species, which are formed at the anodic side. The cathodic current may have also been contributed by the hydrogen evolution reaction (HER: $2H_2O + 2e^- \rightleftharpoons H_2 + 2OH^-$, E vs RHE = 0 V) because the applied potential is more negative than the thermodynamic potential required to reduce a H^+ ion. Besides HER, the oxygen reduction reaction (ORR: $O_2 + 2H_2O + 4e^- \rightleftharpoons 4OH^-$, E vs RHE = 1.23 V) may occur in the entire potential window of −427 to 173 mV because the upper potential is lower than the thermodynamic reduction potential of ORR. These mean, both the HER and the ORR processes can produce hydroxide species at the solid/liquid interfaces, and these hydroxide species can readily react with Fe^{3+}/Ni^{2+} ions and form bimetallic hydroxides on the surfaces of the iron plate. These electrochemical processes can also lead to surface reconstruction on the iron plate as depicted in Scheme 1. In other words, during continuous CV cycles, the iron electrode undergoes repeated cathodic reduction and anodic oxidation, and thus surface reconstruction, finally forming the OER electrodes. The one prepared under most optimal CV cycling (15 cycles) is named FeNiRedox.

In order to understand the effect of cathodic reduction as well as anodic oxidation on the surface reconstruction of the iron plate independent of each other, two other electrodes are synthesized in the potential windows where only cathodic reduction or anodic oxidation is dominant. The resulting electrodes are named as FeNiRed and FeNiOx, respectively. As shown in Figure 1B, during the synthesis of FeNiRed in a potential window from −427 to −77 mV, a cathodic reduction peak at ca. −314 mV forms and then remains stable. Since the electrochemical oxidation of iron does not occur when the applied potential is < −77 mV, as discussed earlier, the peak at ca. −314 mV must be associated with the reduction of some iron containing species present on the iron plate due to aerobic oxidation. In the case of FeNiOx (Figure 1C), the anodic oxidation current increases quickly in the first few cycles and then reaches a steady state in the later cycles. This current is primarily related to the oxidation of metallic iron. On the basis of the applied potential windows mentioned above as well as the thermodynamic reduction potentials of HER and ORR, the sources of hydroxide species in FeNiRed can be HER or ORR and the sources of hydroxide species in FeNiOx can be ORR.

To determine if oxygen is required for the electrochemical activation, an additional electrode is synthesized by the same procedure as the one used to make FeNiRedox, except by bubbling the electrolyte (0.1 M $NiSO_4$) with argon to remove oxygen. The resulting electrode is denoted as FeNiRedox-Ar. Figure 1D displays the 15 CV curves obtained for this material. Unlike the oxidation current given by FeNiRedox (Figure 1A), the one given by FeNiRedox-Ar in the range of −77 to 173 mV decreases when going from the first to 15th cycle (Figure 1D), indicating that the oxidation of the iron plate substantially slows down without oxygen.

In order to check the oxidative dissolution of iron under different applied potentials and measure the amounts of ionic iron species leached into the solution during the electrochemical synthesis, inductively coupled plasma-optical emission spectroscopy (ICP-OES) is used. As shown in Figure S3, the electrolyte after the synthesis of $FeNiO_x$ has the highest concentration of iron (23.09 mg/L). This indicates that the dissolution of iron to the corresponding high oxidation species is prevalent when the applied potential is > −77 mV. The electrolyte in which FeNiRedox is synthesized, in contrast, contains less iron (13.16 mg/L). This implies that a significant amount of iron cations react with hydroxide species and remain on the surfaces of the iron plate when the potential is < −77 mV. Meanwhile, the electrolyte after the preparation of FeNiRed has the least amount of iron (0.33 mg/L), which is however 6.6-fold higher compared with the trace amount of iron (0.05 mg/L) found in a fresh 0.1 M $NiSO_4$ solution. This

https://dx.doi.org/10.1021/acssuschemeng.0c04666
ACS Sustainable Chem. Eng. 2020, 8, 15550−15559

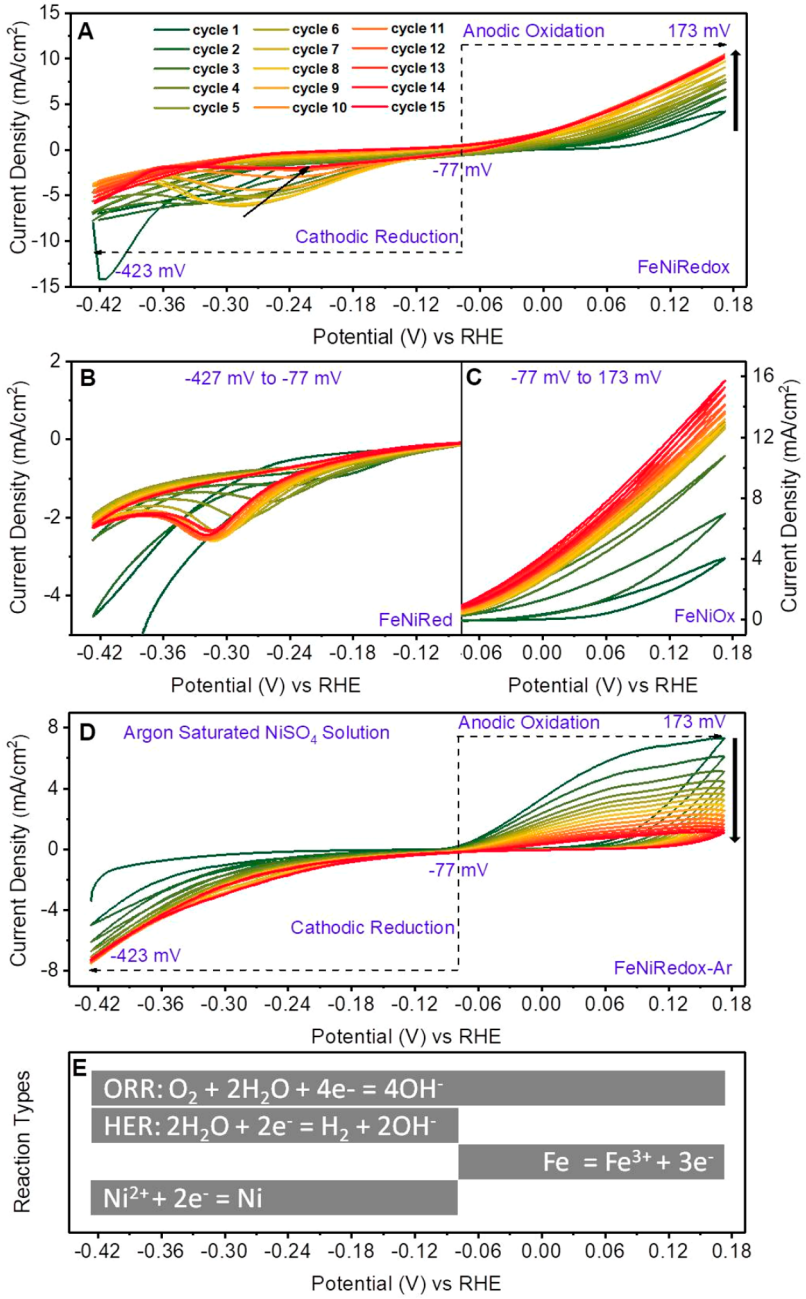

Figure 1. Electrochemical activation of iron plates in 0.1 M $NiSO_4$ solution by running 15 CV cycles at the scan rate of 10 mV/s in different potential windows. The potential windows used for CV cycles are (A) −0.427 to 0.173 V, (B) −0.427 V to −0.077 V, and (C) −0.077 to 0.173 V, and these produce FeNiRedox, FeNiRed, and FeNiOx electrodes, respectively. (D) FeNiRedox-Ar is obtained by cycling an iron plate from −0.427 to 0.173 V in Ar-saturated 0.1 M $NiSO_4$ solution for 15 cycles at a scan rate of 10 mV/s. (E) The major redox reactions that can occur on the electrodes in different applied potential windows are provided.

means that, even in the potential range of −427 to −77 mV, metallic iron leaches into the solution; however, the amount is small compared with the one that leaches into the solution in the potential range of −77 to 173 mV.

These results are corroborated by X-ray photoemission spectroscopy (XPS) (Figures 2 and S2). The oxidation state of the metallic species present on the materials and the possible origins of the current during potential cycling are also determined from the XPS results. The atomic percentages of surface iron with respect to the total surface metal atoms (i.e., Fe + Ni) in FeNiRedox, FeNiRed, and FeNiOx are found to be 35.9%, 17.5%, and 73.8%, respectively. FeNiRed has the lowest amount of iron because iron has less tendency to oxidize when the potential is below −77 mV. FeNiOx has the highest amount of iron because the anodic current from −77 to 173 mV is mainly associated with the oxidative dissolution of iron. In addition, the XPS spectra depicted in Figure 2A show two doublet peaks at binding energies of ca. 712 and 725 eV that correspond to Fe $2p_{3/2}$ and Fe $2p_{1/2}$ of Fe^{3+} species, respectively.[9,31] This indicates the existence of Fe^{3+} on the surfaces of the electrochemically activated iron electrode. Furthermore, a peak at 856.2 eV corresponding to Ni $2p_{3/2}$ of Ni^{2+}, and an associated satellite peak at 861.8 eV, are observed (Figure 2B–D).[10] In the case of the high-resolution XPS

https://dx.doi.org/10.1021/acssuschemeng.0c04666
ACS Sustainable Chem. Eng. 2020, 8, 15550−15559

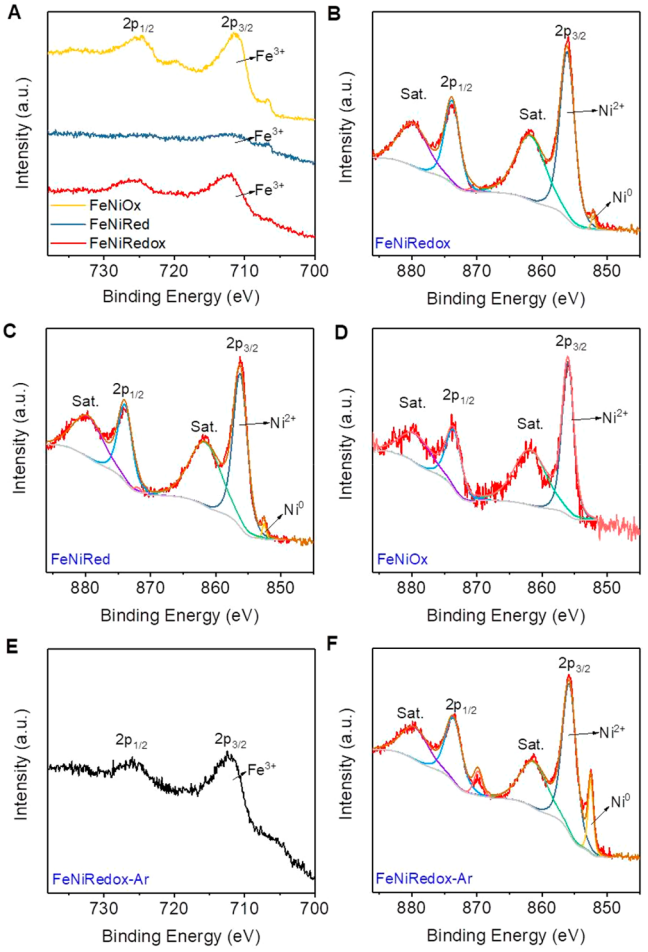

Figure 2. (A) High resolution XPS spectra of Fe 2p peaks of FeNiRedox, FeNiRed, and FeNiOx electrodes. High-resolution XPS spectra of Ni 2p peaks of (B) FeNiRedox, (C) FeNiRed, and (D) FeNiOx electrodes. High-resolution XPS spectra of (E) Fe 2p and (F) Ni 2p peaks of FeNiRedox-Ar electrode.

spectra of Ni 2p peak of FeNiRedox and FeNiRed, besides the major peak at 856.2 eV due to Ni $2p_{3/2}$ of Ni^{2+}, there is a minor one at ca. 852.5 eV due to Ni $2p_{3/2}$ of metallic Ni. The latter peak is absent in the XPS spectra of Ni 2p of FeNiOx. These results suggest that a small portion of the cathodic current in the potential window of −427 to −77 mV must have been due to the formation of metallic Ni. The XPS spectra of O 1s of FeNiRedox and FeNiRed show a single peak at 531.8 eV, indicating the presence of metal−OH species on the materials (Figure S4A,B). For FeNiOx electrode (see Figure S4C,D), in addition to the major peak at 531.8 eV, there is a shoulder at a lower binding energy of 530 eV attributable to metal-O species.[31,32] These data are consistent with our proposed mechanism that the hydroxide species produced during HER and ORR must have reacted with Fe^{3+} and Ni^{2+} cations to form bimetallic hydroxides, $Fe_xNi_y(OH)_z$. The surface composition of FeNiRedox-Ar is also analyzed using XPS (Figure 2E). The Fe 2p signal confirms the presence of Fe^{3+} on the surface of the electrode. The peak for Ni 2p of metallic Ni at ca. 852.5 eV in FeNiRedox-Ar is much stronger compared with the one seen in the spectrum for FeNiRedox (Figure 2F). This reveals that not only a large amount of metallic Ni is present on FeNiRedox-Ar but also the reduction of Ni^{2+} into Ni^0 takes place more readily without competing with ORR during the synthesis of this electrode via potential cycling

Conventional electrodeposition can be either cathodic or anodic. The former is the most commonly used method to deposit metallic hydroxides on conducting substrates. For example, a solution containing metal nitrate can be used as a cathodic deposition electrolyte, where nitrate ions are reduced through the following equation: $NO_3^- + 7H_2O + 8e^- = NH_4^+ + 10OH^-$. The hydroxide ions generated by the reaction can then react with surface metallic species and form metallic hydroxide films on different substrates.[15] Anodic electrodeposition can produce transition metal (oxy)hydroxide thin films through oxidative deposition mechanism with the reaction: $M^{2+}(aq) + 2H_2O = MOOH(s) + e^- + 3H^+$.[33] Our electrochemical activation approach is different from these previously reported electrochemical deposition processes, because both cathodic reduction and anodic oxidation are essential to produce the OER electrode.

SEM images of the as-synthesized electrodes (Figures 3 and S5) show uniformly grown $Fe_xNi_y(OH)_z$ nanosheets on all of them except on FeNiRedox-Ar. The thickness of the nanosheets on FeNiRedox, FeNiRed, and FeNiOx are 18.7 ± 4.5, 18.8 ± 3.7, and 17.9 ± 2.2 nm, respectively. It should be noted that the pores formed in the nanosheets of FeNiRedox are larger than those formed in the nanosheets of the other two electrodes. Such pores can assist with mass transport during electrocatalysis. Transmission electron microscope (TEM) image of FeNiRedox shows a lattice spacing of ca. 0.27 nm, which can be indexed as the (101) facet of FeNi hydroxide (Figure S6).[10] SEM image of FeNiRedox-Ar (Figure 3D) shows a dense film, which appears different from the nanosheet arrays seen in the corresponding electrode prepared in the presence of oxygen. This also explains why the anodic current is decreasing when going from cycle 1 to cycle 15 in the former (Figure 1D), which means the dense film covering the iron surface must have been prohibiting the oxidation of underlying metallic iron further.

XRD patterns of all electrodes (Figure S7) show two major peaks at ca. 44.7° and 65.0°, corresponding to metallic Fe (110) and (200) planes. The XRD patterns of FeNiRedox, FeNiRed, and FeNiRedox-Ar show two peaks, albeit minor ones, at ca. 51.9° and 76.4°, indicating the presence of metallic Ni on these electrodes. The results are consistent with those obtained by XPS analysis. The formation of metallic Ni is due to the electrochemical reaction of $Ni^{2+} + 2e^- = Ni$. For FeNiRedox, there are minor and broad peaks at 2θ of 11.6°, 23.3°, and 34.9°, which can be assigned to the (003), (006), and (012)/(101) signals of FeNi hydroxide, respectively. Other peaks associated with FeNi hydroxide are not observed as the amount of the catalyst (FeNi hydroxide) on the iron plate is small and has low crystallinity. For FeNiRed and FeNiOx electrodes, no peaks associated with FeNi hydroxide are observed, presumably due to the smaller amount of this catalyst on their surfaces and possibly also due to the low crystallinity of the FeNi hydroxide, if any.

Next, linear sweep voltammetry (LSV) curves of OER over activated iron plates synthesized in $NiSO_4$ electrolyte (0.1 M) with different CV cycles are obtained (Figure S8). Comparison of the current densities show that the electrocatalytic performances of FeNiRedox electrodes for OER increases significantly when the cycling number is increased from 5 to 15; however, after 15 cycles, their activity shows only a very minor change/improvement. By taking these into consider-

https://dx.doi.org/10.1021/acssuschemeng.0c04666
ACS Sustainable Chem. Eng. 2020, 8, 15550−15559

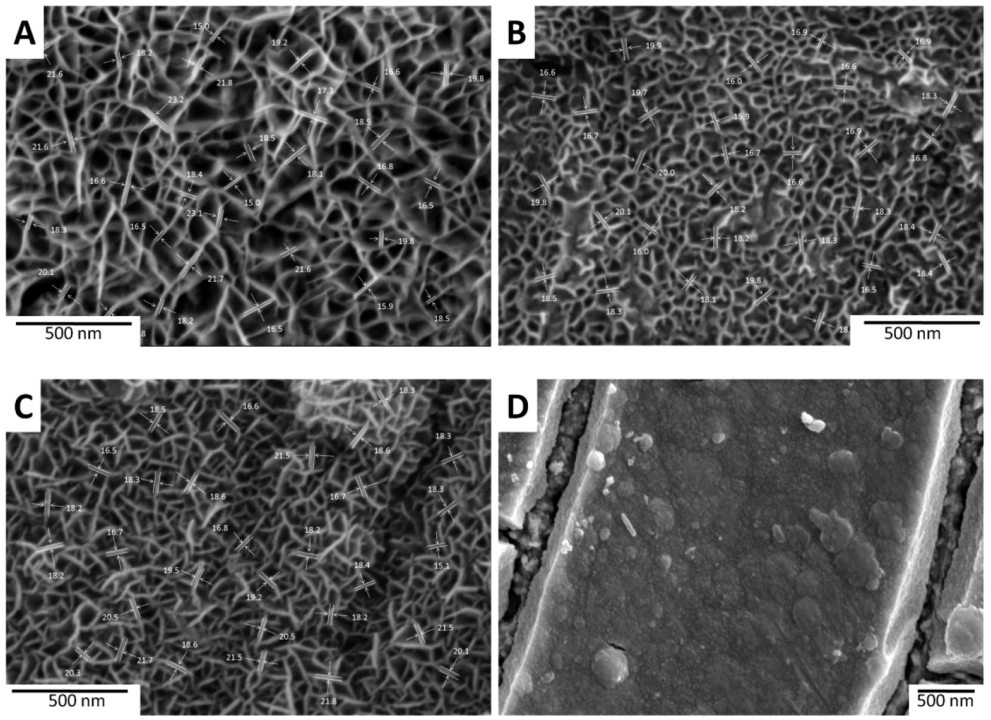

Figure 3. SEM images of (A) FeNiRedox, (B) FeNiRed, (C) FeNiOx, and (D) FeNiRedox-Ar. Larger-sized images for parts A, B, and C showing the measured thicknesses of the frameworks more clearly are also available in Figure S5 in the SI.

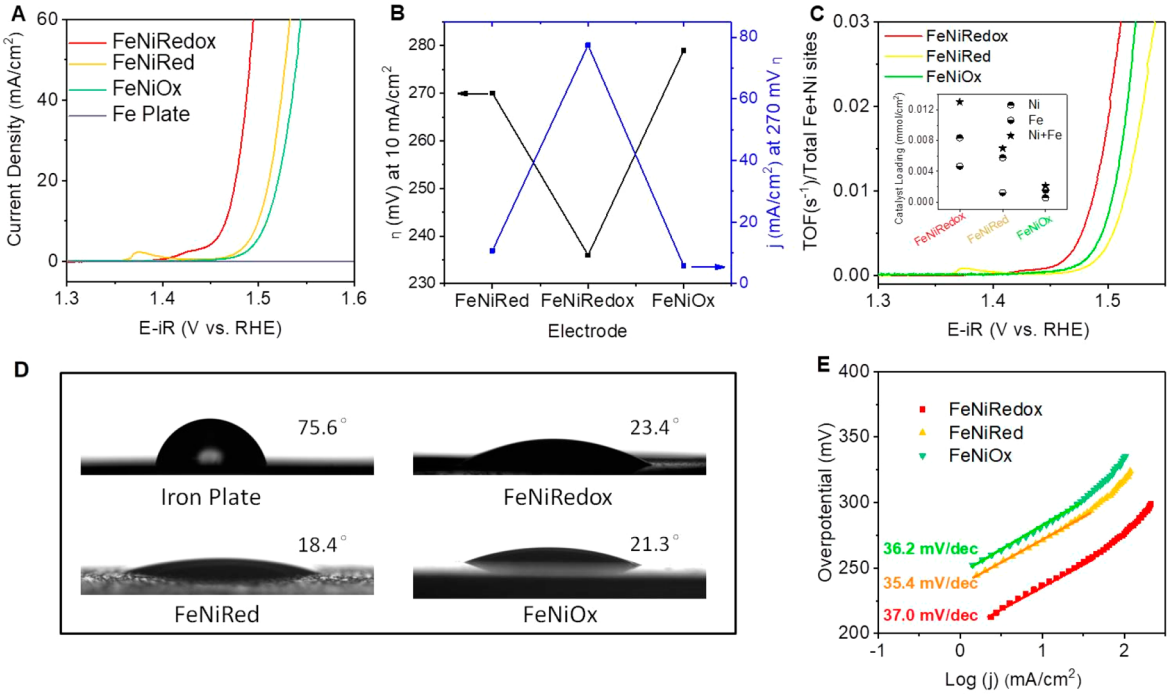

Figure 4. (A) LSV curves of OER in 1 M KOH solution over FeNiRedox, FeNiRed, and FeNiOx at a scan rate of 1 mV/s. (B) Comparison of the overpotentials (η) required by the three electrodes to electrocatalyze OER at a current density of 10 mA/cm^2 and their current densities at 270 mV. (C) Calculated TOFs of FeNiRedox, FeNiRed, and FeNiOx, with the inset showing the loading of active catalyst on each electrode. (D) Contact angles of a fresh iron plate and iron plates after electrochemical activation with 15 CV cycles in 0.1 M $NiSO_4$ solution in different potential windows (namely, FeNiRedox, FeNiRed, and FeNiOx). (E) Tafel plots of OER over FeNiRedox, FeNiRed, and FeNiOx.

ation, the most optimal electrode, which is prepared in 15 cycles or in the shortest possible time via activation of an iron plate (FeNiRedox), was used for further studies. Similarly, the control electrodes were prepared in 15 CV cycles.

The catalytic performances of the electrodes synthesized with 15 cycles for OER are evaluated in 1 M KOH electrolyte via LSV at a slow scan rate of of 1 mV/s to minimize the effect of capacitive current. The results are summarized in Figure 4A,B. Their relative catalytic activities, expressed by the

https://dx.doi.org/10.1021/acssuschemeng.0c04666
ACS Sustainable Chem. Eng. 2020, 8, 15550−15559

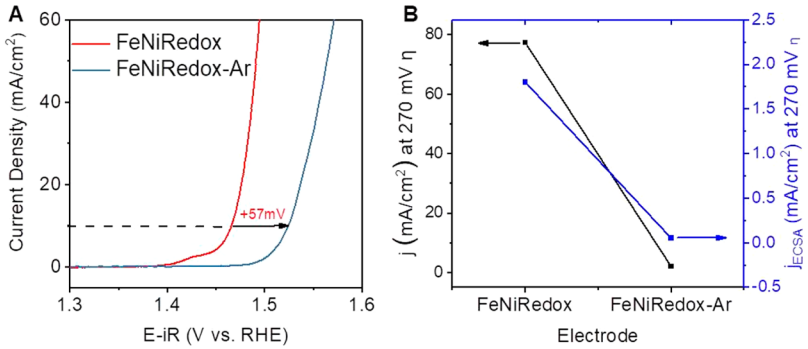

Figure 5. (A) Comparison of LSV curves of OER over of FeNiRedox and FeNiRedox-Ar electrodes. (B) Comparison of the their catalytic activities for OER as normalized by their geometrical surface area (black curve) and (blue curve).

overpotentials they require to catalyze OER at a geometric current density of 10 mA/cm^2, are FeNiRedox (236 mV) > FeNiRed (270 mV) > FeNiOx (279 mV). It is also worth adding here that at an overpotential of 270 mV, FeNiRedox achieves a current density of 77.4 mA/cm^2, which is 7.2-fold and 13.4-fold higher than the values obtained for FeNiRed and FeNiOx, respectively. These results indicate that FeNiRedox is the most active electrode for OER. This also highlights the importance in selecting the right potential window to electrochemically activate and convert iron into highly OER active bimetallic hydroxides with optimized Fe/Ni composition.[31,34] Consistent with this result, the Nyquist plots reveal the lowest charge-transfer resistance in FeNiRedox (Figure S9), suggesting that this electrode can provide the fastest charge transfer rate during OER. In order to compare the intrinsic catalytic activities, the loadings of catalytic active groups on the surfaces of the electrodes are measured and compiled in the inset of Figure 4C. It is clear that FeNiRedox has a higher catalyst loading compared with the two other electrodes. Assuming all the Fe and Ni sites are the active centers driving the OER, the TOF calculated based on both metals confirms that FeNiRedox still has the highest intrinsic activity among all these electrodes (Figure 4C). In addition, FeNiRedox has the highest mass activity compared with the other two electrodes (Figure S10).

It should be emphasized that the iron plate treated with electrochemical activation in $NiSO_4$ electrolyte for 30 min (FeNiRedox) shows a very high catalytic activity for OER while the pure iron plate (before activation) barely shows any activity. To investigate whether Ni^{2+} is necessary for the formation of efficient OER electrode, an additional control electrode is synthesized by running 15 CV cycles on an iron plate in 0.1 M Na_2SO_4 (instead of $NiSO_4$) electrolyte (Figure S11). The electrode displays slightly improved activity compared with a fresh iron plate, but its performance is far inferior to that of FeNiRedox. (Figure S12). This result indicates that nickel plays a very essential role in improving the electrocatalytic activity of the electrode for OER. In fact, the concentration of Ni^{2+} used for activating the iron plate matters based on the additional study we have conducted. Two more electrodes electrochemically activated using lower concentrations of $NiSO_4$ are synthesized under similar condition as FeNiRedox. The LSV curves of OER over the electrodes synthesized in 0.001, 0.01, and 0.1 M $NiSO_4$ electrolytes (Figure S13) shows that the overpotentials required by the electrodes to catalyze the reaction with a geometric current density of 10 mA/cm^2 are 281, 242, and 236 mV, respectively. This result indicates that higher concentrations of Ni^{2+} favors the electrochemical activation of iron into more active OER electrodes.

The contact angles of FeNiRedox electrode and iron plate are measured to study their surface hydrophobicity or hydrophilicity. As shown in Figure 4D, after electrochemical activation, the surface of FeNiRedox becomes more hydrophilic with a contact angle of 23.4°, which is much lower than that of the original iron plate, whose contact angle is 75.6°. This must be due to the hydroxyl groups present on the surfaces of FeNiRedox. This hydrophilic property is beneficial for electrocatalysis in aqueous and polar electrolytes as it allows electrolytes to interact with the surfaces of catalysts better.[35] The contact angles of FeNiRed and FeNiOx are found to be close to that of FeNiRedox.

To explore the OER kinetics over the materials, the Tafel slopes are determined by plotting the OER overpotential versus current density in logarithmic scale. As shown in Figure 4E, the Tafel slopes of FeNiRedox, FeNiRed, and FeNiOx are 37.0, 35.4, and 36.2 mV/dec, respectively. The results suggest that the differences in the transition metal composition of these Fe−Ni-based electrocatalysts do not lead to significant differences in their Tafel slopes. Moreover, the values are consistent with the Tafel slope of ca. 40 mV/dec reported for OER over FeNi films by other research groups.[31,34] The fact that the three catalysts studied herein have similar Tafel slopes indicates that the OER processes over them have a similar rate-determining step. OER in basic solution can be described with the following four elementary steps (eqs 5−8)[36]

$$* + OH^- \rightleftharpoons OH^* + e^- \quad (5)$$

$$OH^* + OH^- \rightleftharpoons O^* + H_2O + e^- \quad (6)$$

$$O^* + OH^- \rightleftharpoons OOH^* + e^- \quad (7)$$

$$OOH^* + OH^- \rightleftharpoons * + O_2 + H_2O + e^- \quad (8)$$

where * in the equations represents the catalytic active site on the catalyst's surface. A Tafel slope close to 40 mV/dec implies that the second step of O* intermediate formation ($OH^* + OH^- = O^* + H_2O + e^-$) is the rate-determining step of OER over the three electrodes.[32]

The LSV curves in Figure 5A show that FeNiRedox-Ar needs an overpotential of 293 mV to catalyze OER with a current density of 10 mA/cm^2, which is 57 mV higher than that of FeNiRedox. This indicates that the presence of oxygen during potential cycling plays an important role in the formation of the highly active Fe−Ni-based OER catalyst. FeNiRedox's high OER activity is also evidenced by its high

https://dx.doi.org/10.1021/acssuschemeng.0c04666
ACS Sustainable Chem. Eng. 2020, 8, 15550−15559

specific activity: an activity normalized by the electrochemical active surface area (ECSA) of the material. ESCA of the electrodes are obtained from the double layer capacitances of the materials (Figure S14). Meanwhile, as shown in Figure 5B, the specific activity of FeNiRedox at an overpotential of 270 mV is 1.8 mA/cm^2, which is about 33-times higher than that of FeNiRedox-Ar (0.054 mA/cm^2). This means, FeNiRedox has a higher catalytic activity compared with FeNiRedox-Ar. This is because, in the absence of oxygen, the nickel cations can be reduced to metallic nickel and deposit on the iron surface. (Note that metallic nickel has much lower catalytic activity compared with FeNi hydroxides). As shown in Table S1, FeNiRedox-Ar has the highest percentage of Ni(0) out of the total Ni present in the electrode, as determined by XPS analysis. In the case of FeNiRedox, the presence of oxygen helps with the formation of the more catalytically active FeNi hydroxide on the substrate.

Besides excellent catalytic activity, stability is another important requirement that OER catalysts should meet in order find practical applications. The stability of FeNiRedox electrode is tested in 1 M KOH solution. Remarkably, the electrode remains stable while catalyzing OER at a high current density of 100 mA/cm^2 for, at least, 72 h (Figure 6A). In addition, the amount of O_2 evolved is in agreement with the theoretically calculated O_2 (Figure 6B), suggesting a near 100% Faradaic efficiency. The ability to catalyze OER at high current density is important for practical applications. As shown in Figure S15, FeNiRedox can do so at a current density of 1000 mA/cm^2 while remaining stable for, at least, 24 h. During the course of chronopotentiometric measurement at 1000 mA/cm^2, the electrolyte was sampled at 0, 2, 4, and 20 h for ICP-MS analysis to probe the possible leaching of metal during OER catalysis. As shown in Table S2, the amount of leached iron is below 1 mg/L even after 20 h operation, further suggesting that FeNiRedox is stable during OER. The SEM image of FeNiRedox electrode after 24 h operation at high current density (1000 mA/cm^2) is compared with that of the original electrode before electrocatalysis (Figure S16). The images show that the structure and morphology of the electrode remains almost unchanged. This results, coupled with its stable electrocatalytic activity, indicate the stability of FeNiRedox electrode during OER.

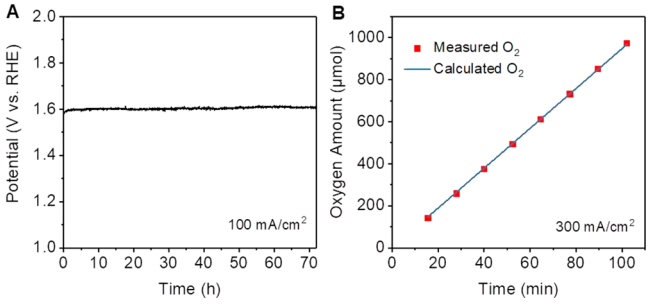

Figure 6. (A) Chronopotentiometric curve of OER over FeNiRedox for 70 hours at a constant current density of 100 mA/cm^2 without *iR*-correction. (B) Comparison of theoretically calculated and experimentally measured O_2 evolved by OER.

A previous study showed that the *corrosion* of iron plate in $NiSO_4$ solution after 12 h would lead to a Ni-Fe-based electrocatalyst for OER.[18] To confirm the major contribution of *electrochemical activation* in our case, an additional control material was prepared by immersing the iron plate in 0.1 M $NiSO_4$ solution (or a corrosion experiment) under ambient conditions for 30 min, or the same amount of time needed for the electrochemical activation synthesis. The LSV curves in Figure S17 indicate that the electrode prepared without electrochemical activation requires a much higher overpotential to give the same current density than FeNiRedox. This further proves that the *electrochemical activation* is critical in the formation of this highly active OER electrode in a much shorter time. Moreover, in terms of the overpotential required to generate a current density of 10 mA/cm^2 in OER, the catalytic activity of FeNiRedox is comparable with those of other notable recently reported electrocatalysts (see Table S3).

CONCLUSIONS

In summary, we have developed a facile electrochemical method to synthesize efficient and stable OER electrodes using an inexpensive iron plate via CV cycling in $NiSO_4$ solution. The iron plate underwent compositional and structural changes during successive CV cycling and accompanying electrochemical processes. In the process, surface metallic iron was oxidized and transformed into Fe^{3+} species, particularly when the potential was higher than −77 mV. Meanwhile, the ORR in the potential window of −437 to 173 mV and the HER at a potential of less than −77 mV produced hydroxide anions that then reacted with the Ni^{2+} ions present in the electrolyte and with the Fe^{3+} ions leached from the iron plate. This process ultimately formed electrocatalytically active bimetallic hydroxides on the surfaces of the iron plate. We have also shown that the potential range for electrochemical activation would play an important role in generating this highly active OER electrode, and the presence of oxygen during the activation process was vital for improving the electrode's catalytic performances in OER. The electrode obtained under optimal conditions (FeNiRedox) demonstrated a high catalytic activity for OER, requiring an overpotential of 236 mV to catalyze the reaction at a current density of 10 mA/cm^2. It also remained stable for at least 72 h at a current density of 100 mA/cm^2. Its catalytic activity, stability, and the facile synthetic method and inexpensive iron substrate it involves make this electrode attractive for water electrolyzers. Furthermore, this novel method could be further extended to synthesize other catalytic films with different compositions from iron plates or other substrates.

ASSOCIATED CONTENT

Supporting Information

The Supporting Information is available free of charge at https://pubs.acs.org/doi/10.1021/acssuschemeng.0c04666.

Reference electrode calibration curve, photograph of electrodes, ICP-OES data, high resolution XPS curves, SEM images, HRTEM image, Nyquist plots, XRD patterns and electrochemical data (PDF)

AUTHOR INFORMATION

Corresponding Authors

Xiaoxi Huang − *Hoffmann Institute of Advanced Materials, Shenzhen Polytechnic, Shenzhen 518055, PR China;* orcid.org/0000-0002-1975-2312; Email: xiaoxihuang@szpt.edu.cn

Tewodros Asefa − *Department of Chemistry and Chemical Biology, Rutgers and Department of Chemical and Biochemical*

https://dx.doi.org/10.1021/acssuschemeng.0c04666
ACS Sustainable Chem. Eng. 2020, 8, 15550−15559

Engineering, Rutgers, The State University of New Jersey, Piscataway, New Jersey 08854, United States; orcid.org/0000-0001-8634-5437; Email: tasefa@chem.rutgers.edu

Authors

Shiyu Liu − *Hoffmann Institute of Advanced Materials, Shenzhen Polytechnic, Shenzhen 518055, PR China*

Jian Zhang − *Hoffmann Institute of Advanced Materials, Shenzhen Polytechnic, Shenzhen 518055, PR China; School of Chemistry and Chemical Engineering, South China University of Technology, Guangzhou 510640, PR China*

Hao Wang − *Hoffmann Institute of Advanced Materials, Shenzhen Polytechnic, Shenzhen 518055, PR China;* orcid.org/0000-0001-7732-778X

Complete contact information is available at: https://pubs.acs.org/10.1021/acssuschemeng.0c04666

Notes

The authors declare no competing financial interest.

■ ACKNOWLEDGMENTS

We thank Shenzhen Polytechnic for supporting the work and for the Postdoctoral Foundation Project of Shenzhen Polytechnic, 6020330007K.

■ REFERENCES

(1) Burke, M. S.; Enman, L. J.; Batchellor, A. S.; Zou, S.; Boettcher, S. W. Oxygen evolution reaction electrocatalysis on transition metal oxides and (oxy)hydroxides: activity trends and design principles. *Chem. Mater.* **2015**, *27* (22), 7549−7558.

(2) Cai, Z.; Bu, X.; Wang, P.; Ho, J. C.; Yang, J.; Wang, X. Recent advances on layered double hydroxide electrocatalysts for oxygen evolution reaction. *J. Mater. Chem. A* **2019**, *7* (10), 5069−5089.

(3) Hunter, B. M.; Gray, H. B.; Müller, A. M. Earth-abundant heterogeneous water oxidation catalysts. *Chem. Rev.* **2016**, *116* (22), 14120−14136.

(4) Gao, R.; Yan, D. Recent development of Ni/Fe-based micro/nanostructures toward photo/electrochemical water oxidation. *Adv. Energy Mater.* **2020**, *10* (11), 1900954.

(5) Zhang, W.; Li, D.; Zhang, L.; She, X.; Yang, D. NiFe-based nanostructures on nickel foam as highly efficiently electrocatalysts for oxygen and hydrogen evolution reactions. *J. Energy Chem.* **2019**, *39*, 39−53.

(6) Guo, F.; Wu, Y.; Chen, H.; Liu, Y.; Yang, L.; Ai, X.; Zou, X. High-performance oxygen evolution electrocatalysis by boronized metal sheets with self-functionalized surfaces. *Energy Environ. Sci.* **2019**, *12* (2), 684−692.

(7) Li, J.; Chen, H.; Liu, Y.; Gao, R.; Zou, X. In situ structural evolution of nickel boride catalyst towards synergistic geometric and electronic optimization of oxygen evolution reaction. *J. Mater. Chem. A* **2019**, *7* (10), 5288−5294.

(8) Li, R.; Wang, Y.; Li, W.; Zhou, S.; Tian, P.; Gao, H.; Liu, X.; Zang, J. Ternary NiFeZr layered double hydroxides: a highly efficient catalyst for the oxygen evolution reaction. *Chem. Commun.* **2019**, *55* (89), 13370−13373.

(9) Qi, Y. F.; Wang, Q.; Wang, X. G.; Liu, Z. Y.; Zhao, X. J.; Yang, E. C. Self-supported Co-doped FeNi carbonate hydroxide nanosheet array as a highly efficient electrocatalyst towards the oxygen evolution reaction in an alkaline solution. *Nanoscale* **2019**, *11* (22), 10595−10602.

(10) Zhang, B.; Jiang, K.; Wang, H.; Hu, S. Fluoride-induced dynamic surface self-reconstruction produces unexpectedly efficient oxygen-evolution catalyst. *Nano Lett.* **2019**, *19* (1), 530−537.

(11) Ma, Y.; Wang, Y.; Xie, D.; Gu, Y.; Zhang, H.; Wang, G.; Zhang, Y.; Zhao, H.; Wong, P. K. NiFe-layered double hydroxide nanosheet arrays supported on carbon cloth for highly sensitive detection of nitrite. *ACS Appl. Mater. Interfaces* **2018**, *10* (7), 6541−6551.

(12) Liu, J.; Zheng, Y.; Wang, Z.; Lu, Z.; Vasileff, A.; Qiao, S.-Z. Free-standing single-crystalline NiFe-hydroxide nanoflake arrays: a self-activated and robust electrocatalyst for oxygen evolution. *Chem. Commun.* **2018**, *54* (5), 463−466.

(13) Bose, R.; Karuppasamy, K.; Rajan, H.; Velusamy, D. B.; Kim, H.-S.; Alfantazi, A. Electrodeposition of unary oxide on a bimetallic dydroxide as a highly active and stable catalyst for water oxidation. *ACS Sustainable Chem. Eng.* **2019**, *7* (19), 16392−16400.

(14) Li, Z.; Shao, M.; An, H.; Wang, Z.; Xu, S.; Wei, M.; Evans, D. G.; Duan, X. Fast electrosynthesis of Fe-containing layered double hydroxide arrays toward highly efficient electrocatalytic oxidation reactions. *Chem. Sci.* **2015**, *6* (11), 6624−6631.

(15) Lu, X.; Zhao, C. Electrodeposition of hierarchically structured three-dimensional nickel−iron electrodes for efficient oxygen evolution at high current densities. *Nat. Commun.* **2015**, *6*, 6616.

(16) Wang, P.; Lin, Y.; Wan, L.; Wang, B. Construction of a janus MnO_2-NiFe electrode via selective electrodeposition strategy as a high-performance bifunctional electrocatalyst for rechargeable zinc−air batteries. *ACS Appl. Mater. Interfaces* **2019**, *11* (41), 37701−37707.

(17) Zhang, J.; Bai, Y.; Zhang, C.; Gao, H.; Niu, J.; Shi, Y.; Zhang, Y.; Song, M.; Zhang, Z. Hybrid $Ni(OH)_2$/FeOOH@NiFe nanosheet catalysts toward highly efficient oxygen evolution reaction with ultralong stability over 1000 h. *ACS Sustainable Chem. Eng.* **2019**, *7* (17), 14601−14610.

(18) Liu, Y.; Liang, X.; Gu, L.; Zhang, Y.; Li, G. D.; Zou, X.; Chen, J. S. Corrosion engineering towards efficient oxygen evolution electrodes with stable catalytic activity for over 6000 h. *Nat. Commun.* **2018**, *9*, 2609.

(19) Liu, J.; Zheng, Y.; Jiao, Y.; Wang, Z.; Lu, Z.; Vasileff, A.; Qiao, S.-Z. NiO as a bifunctional promoter for RuO_2 toward superior overall water splitting. *Small* **2018**, *14* (16), 1704073.

(20) Liu, J.; Wang, Z.; Su, K.; Xv, D.; Zhao, D.; Li, J.; Tong, H.; Qian, D.; Yang, C.; Lu, Z. Self-supported hierarchical IrO_2@NiO nanoflake arrays as an efficient and durable catalyst for electrochemical oxygen evolution. *ACS Appl. Mater. Interfaces* **2019**, *11* (29), 25854−25862.

(21) Zhang, J.; Liu, J.; Xi, L.; Yu, Y.; Chen, N.; Sun, S.; Wang, W.; Lange, K. M.; Zhang, B. Single-atom Au/NiFe layered double hydroxide electrocatalyst: probing the origin of activity for oxygen evolution reaction. *J. Am. Chem. Soc.* **2018**, *140* (11), 3876−3879.

(22) Liu, J.; Zhu, D.; Ling, T.; Vasileff, A.; Qiao, S.-Z. S-$NiFe_2O_4$ ultra-small nanoparticle built nanosheets for efficient water splitting in alkaline and neutral pH. *Nano Energy* **2017**, *40*, 264−273.

(23) He, K.; Tadesse Tsega, T.; Liu, X.; Zai, J.; Li, X. H.; Liu, X.; Li, W.; Ali, N.; Qian, X. Utilizing the space-charge region of FeNi-LDH/CoP p−n junction to promote the performance in oxygen evolution electrocatalysis. *Angew. Chem., Int. Ed.* **2019**, *58* (34), 11903−11909.

(24) Subbaraman, R.; Tripkovic, D.; Chang, K.-C.; Strmcnik, D.; Paulikas, A. P.; Hirunsit, P.; Chan, M.; Greeley, J.; Stamenkovic, V.; Markovic, N. M. Trends in activity for the water electrolyser reactions on 3d M(Ni,Co,Fe,Mn) hydr(oxy)oxide catalysts. *Nat. Mater.* **2012**, *11*, 550−557.

(25) Mitra, P. T. D.; Malkhandi, S.; Mecklenburg, M.; Heald, S. M.; Balasubramanian, M.; Narayanan, S. R. An efficient and robust surface-modified iron electrode for oxygen evolution in alkaline water electrolysis. *J. Electrochem. Soc.* **2018**, *165* (5), F392.

(26) Liu, X.; Gong, M.; Xiao, D.; Deng, S.; Liang, J.; Zhao, T.; Lu, Y.; Shen, T.; Zhang, J.; Wang, D. Turning waste into treasure: regulating the oxygen corrosion on Fe foam for efficient electrocatalysis. *Small* **2020**, *16* (24), 2000663.

(27) Yang, X.; Chen, Q. Q.; Wang, C. J.; Hou, C. C.; Chen, Y. Substrate participation ultrafast synthesis of amorphous NiFe nanosheets on iron foam at room temperature toward highly efficient oxygen evolution reaction. *J. Energy Chem.* **2019**, *35*, 197−203.

(28) Stevens, M. B.; Enman, L. J.; Batchellor, A. S.; Cosby, M. R.; Vise, A. E.; Trang, C. D. M.; Boettcher, S. W. Measurement

techniques for the study of thin film heterogeneous water oxidation electrocatalysts. *Chem. Mater.* **2017**, *29* (1), 120−140.
(29) Zhang, C.; Huang, Y.; Yu, Y.; Zhang, J.; Zhuo, S.; Zhang, B. Sub-1.1 nm ultrathin porous CoP nanosheets with dominant reactive {200} facets: a high mass activity and efficient electrocatalyst for the hydrogen evolution reaction. *Chem. Sci.* **2017**, *8* (4), 2769−2775.
(30) Wei, C.; Rao, R. R.; Peng, J.; Huang, B.; Stephens, I. E. L.; Risch, M.; J, Xu. Z.; Shao-Horn, Y. Recommended practices and benchmark activity for hydrogen and oxygen electrocatalysis in water splitting and fuel cells. *Adv. Mater.* **2019**, *31* (31), 1806296.
(31) Louie, M. W.; Bell, A. T. An investigation of thin-film Ni−Fe oxide catalysts for the electrochemical evolution of oxygen. *J. Am. Chem. Soc.* **2013**, *135* (33), 12329−12337.
(32) Burke, M. S.; Kast, M. G.; Trotochaud, L.; Smith, A. M.; Boettcher, S. W. Cobalt−iron (oxy)hydroxide oxygen evolution electrocatalysts: the role of structure and composition on activity, stability, and mechanism. *J. Am. Chem. Soc.* **2015**, *137* (10), 3638−3648.
(33) Morales-Guio, C. G.; Liardet, L.; Hu, X. Oxidatively electrodeposited thin-film transition metal (oxy)hydroxides as oxygen evolution catalysts. *J. Am. Chem. Soc.* **2016**, *138* (28), 8946−8957.
(34) Görlin, M.; Ferreira de Araújo, J.; Schmies, H.; Bernsmeier, D.; Dresp, S.; Gliech, M.; Jusys, Z.; Chernev, P.; Kraehnert, R.; Dau, H.; Strasser, P. Tracking catalyst redox states and reaction dynamics in Ni−Fe oxyhydroxide oxygen evolution reaction electrocatalysts: the role of catalyst support and electrolyte pH. *J. Am. Chem. Soc.* **2017**, *139* (5), 2070−2082.
(35) Liu, J.; Yuan, H.; Wang, Z.; Li, J.; Yang, M.; Cao, L.; Liu, G.; Qian, D.; Lu, G. Self-supported nickel iron oxide nanospindles with high hydrophilicity for efficient oxygen evolution. *Chem. Commun.* **2019**, *55* (73), 10860−10863.
(36) Vij, V.; Sultan, S.; Harzandi, A. M.; Meena, A.; Tiwari, J. N.; Lee, W.-G.; Yoon, T.; Kim, K. S. Nickel-based electrocatalysts for energy-related applications: oxygen reduction, oxygen evolution, and hydrogen evolution reactions. *ACS Catal.* **2017**, *7* (10), 7196−7225.

https://dx.doi.org/10.1021/acssuschemeng.0c04666
ACS Sustainable Chem. Eng. 2020, 8, 15550−15559